A Quantum Mechanics/Molecular Mechanics Study of the Catalytic Mechanism of the Thymidylate Synthase†

Natalia Kanaan, Sergio Martí,* and Vicent Moliner*

Departament de Química Física i Analítica, Universitat Jaume I, 12071 Castellón, Spain

Amnon Kohen

Department of Chemistry, University of Iowa, Iowa City, Iowa 52242

Received September 20, 2006; Revised Manuscript Received January 2, 2007

ABSTRACT: A theoretical study of the molecular mechanism of the thymidylate synthase-catalyzed reaction has been carried out using hybrid quantum mechanics/molecular mechanics methods. We have examined all of the stationary points (reactants, intermediates, transition structures, and products) on the multidimensional potential energy surfaces for the multistep enzymatic process. The characterization of these relevant structures facilitates the gaining of insight into the role of the different residues in the active site. Furthermore, analysis of the full energy profile has revealed that the step corresponding to the reduction of the exocyclic methylene intermediate by hydride transfer from the 6S position of 5,6,7,8-tetrahydrofolate (H_4folate), forming dTMP and 7,8-dihydrofolate (H_2folate), is the rate-limiting step, in accordance with the experimental data. In this step, the hydride transfer and the scission of an overall conserved active site cysteine residue (Cys146 in *Escherichia coli*) take place in a concerted but very asynchronous way. These findings have also been tested with primary and secondary deuterium, tritium, and sulfur kinetic isotope effects, and the calculations have been compared to experimental data. Finally, the incorporation of high-level quantum mechanical corrections to the semiempirical AM1 Hamiltonian into our hybrid scheme has allowed us to obtain reasonable values of the energy barrier for the rate-limiting step. The resulting picture of the complete multistep enzyme mechanism that is obtained reveals several new features of substantial mechanistic interest.

Thymidylate synthase (TS,[1] EC 2.1.1.45) is a symmetric dimer of two subunits formed by 264 amino acids (*Escherichia coli*) with one active site per subunit (*1*). TS catalyzes the reductive methylation of 2′-deoxyuridine 5′-monophosphate (dUMP) using 5,10-methylene-5,6,7,8-tetrahydrofolate (CH_2H_4folate) as a methylene donor and hydride reductant to form 2′-deoxythymidine 5′-monophosphate (dTMP) and 7,8-dihydrofolate (H_2folate). The overall reaction is depicted in Scheme 1. This enzyme, together with dihydrofolate reductase (DHFR) and serine hydroxymethyl transferase (SHMT), forms part of a cycle that replenishes the CH_2H_4-folate. DHFR reduces H_2folate to regenerate H_4folate, using NADPH as a cofactor; meanwhile, SHMT catalyzes the interconversion from serine to glycine, transforming the H_4-folate to CH_2H_4folate. TS is crucial for DNA biosynthesis, because dTMP is one of the building blocks of DNA. Also, since cancerous cells exhibit uncontrolled replication, TS inhibition is an interesting target in the rational design of anticancer drugs. Indeed, there are inhibitors for this enzyme, like 5-FU (5-fluorouracil), which is metabolized by a kinase to its 5′-phosphate and has been proven to be highly active against solid tumors such as those of the breast, head, neck, and colon. However, to inhibit TS in tumor cells, where an increase in its expression levels is detected, a high concentration of the anticancer drug is needed. Unfortunately, this

Scheme 1: Overall Reaction Catalyzed by TS[a]

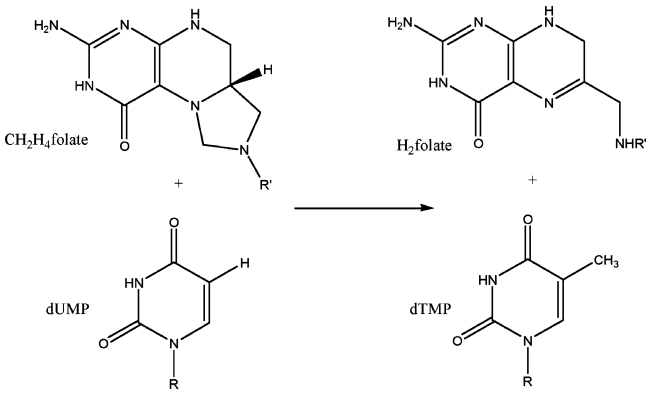

[a] R = 2′-deoxyribose 5′-phosphate, and R′ = PABA glutamate.

† We are grateful to the DGI for Project CTQ2006-15447-C02-01/BQU, to the UJI-BANCAIXA foundation for Project P1·1B2005-13, and to Generalitat Valenciana for Project GV06/152, for NIH Grant R01 GM65368-01, and for NSF Grant CHE-0133117. N.K. acknowledges a doctoral fellowship of the UJI-BANCAIXA foundation.

* To whom correspondence should be addressed. S.M.: e-mail, smarti@uji.es; phone, (+34) 964-728071; fax, (+34) 964-728066. V.M.: e-mail, moliner@uji.es; phone, (+34) 964-728084; fax, (+34) 964-728066.

[1] Abbreviations: TS, thymidylate synthase; QM/MM, quantum mechanics/molecular mechanics; dUMP, 2′-deoxyuridine 5′-monophosphate; dTMP, 2′-deoxythymidine 5′-monophosphate; H_2folate, 7,8-dihydrofolate; CH_2H_4folate, 5,10-methylene-5,6,7,8-tetrahydrofolate; 5-FU, 5-fluorouracil; DFT, density functional theory; KIE, kinetic isotope effect; IRC, intrinsic reaction coordinate path.

10.1021/bi061953y CCC: $37.00
Published on Web 03/01/2007

Scheme 2: Chemical Mechanism for the *E. coli* TS-Catalyzed Reaction Proposed by Carreras and Santi (*1*)[a]

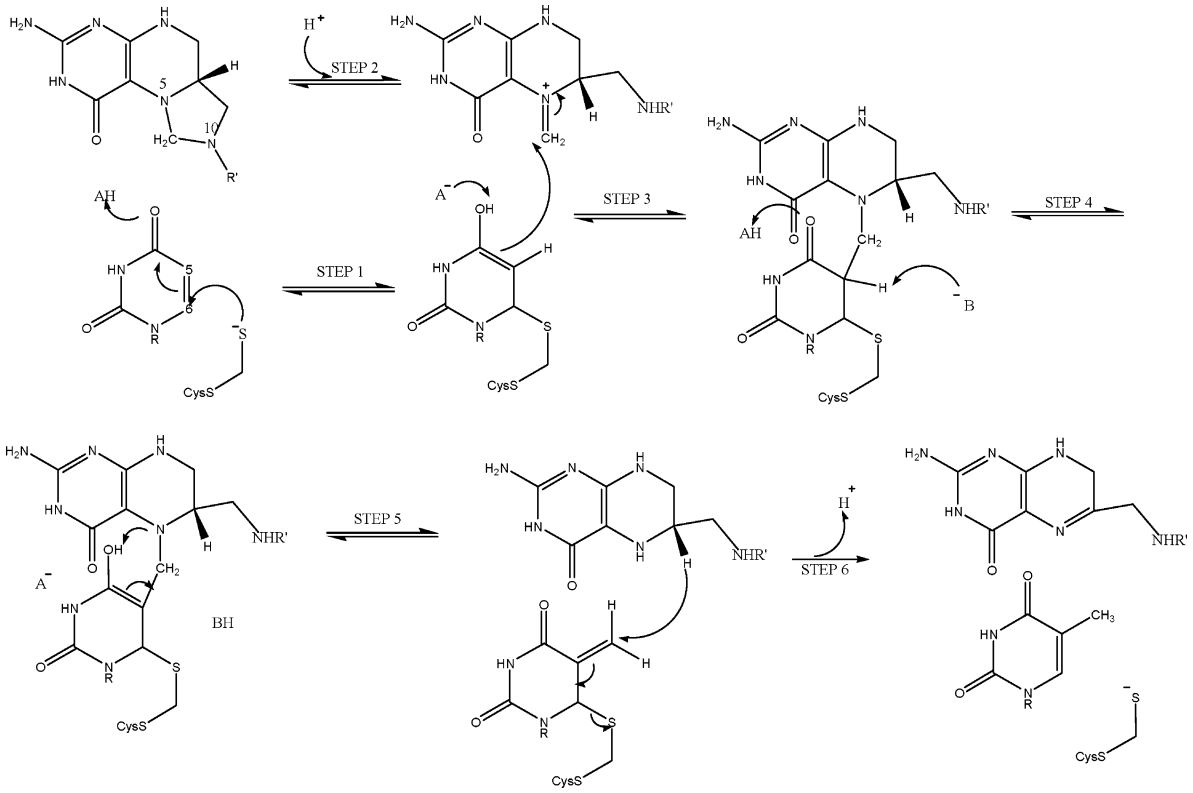

[a] R = 2′-deoxyribose 5′-phosphate, and R′ = PABA glutamate.

excess also damages healthy tissues, resulting in toxicity. This makes it difficult to realize effective treatments without side effects and to avoid the development of drug resistance (*2*). All of these facts provide evidence of the importance of knowing the molecular mechanism of TS in detail for the development of new inhibitors that could act specifically against tumor cells.

The new mechanistic details proposed in this work may indicate new leads to mechanism-based inhibitors and rational drug design. There is another interesting feature in this reaction mechanism, the double action of the folate, both as a donor of methylene and as a reductant. Many studies have been devoted to the elucidation of this mechanism, from the first one proposed by Friedkin in 1959 (*3*) to the prolific work of Santi and co-workers (*4*−*8*). Knowledge of the complete amino acid sequence of *Lactobacillus casei* TS, together with the X-ray crystal structure, information derived from site-directed mutagenesis techniques, and the kinetic isotope effects (KIEs) have provided the basis for a putative mechanism in which TS catalyzes the transfer of a methylene group from CH_2H_4folate to dUMP, followed by the reduction of the methylene to yield dTMP and H_2folate. In this mechanism, as proposed by Carreras and Santi (see Scheme 2) (*1*), the first step consists of the nucleophilic attack by a thiol of a conserved Cys (Cys146 in *E. coli* TS) on C6 of dUMP. Then, C5 of the activated enol binds to the cofactor, which was previously activated by the formation of an iminium ion at N5 (step 2), to form an enzyme-bound covalent intermediate. This step is followed by the abstraction of a proton from C5 of dUMP which leads to the elimination of H_4folate in forming an exocyclic methylene intermediate. Finally, this intermediate is reduced by a transfer of hydride from the 6S position of H_4folate to form products, dTMP and H_2folate.

This proposed mechanism leaves some questions open. For example, what are the source and the destination of some of the protons involved in the mechanism? Another aspect to analyze is which of the steps proceeds via a concerted mechanism and which via a stepwise mechanism; for example, the last step could occur by means of the formation of an enolic intermediate or in an S_N2 fashion.

Kinetic experiments, such as studies of temperature dependency, cofactor inhibition, determination of activation parameters of the rate constants, and measures of intrinsic KIEs, have demonstrated that the rate-determining step of the reaction is the hydride transfer (step 6 in Scheme 2). Some of these studies have also revealed the contribution of vibrationally enhanced quantum mechanical tunneling to the hydride step in the TS-catalyzed reaction (*2*). Nevertheless, as pointed out by Kohen et al., no specific model developed to explain the catalytic role of the residues of the enzyme in this step or its temperature-independent KIEs seems to be completely successful (*2*).

In this study, we have used hybrid QM/MM methods, which combine the reliability of the QM methods and the computational efficiency of the MM methods, to study the full molecular mechanism of the reaction catalyzed by the TS, with special attention to the hydride transfer step.

COMPUTATIONAL METHODS

The starting geometry was obtained from the X-ray crystal structure of the ternary complex of *E. coli* TS with dUMP and a powerful anti-folate inhibitor, 10-propargyl-5,8-dideazafolate (CB3717, PDB entry 2TSC) (*9*−*11*). Once the

Scheme 3: Atom Labeling for the Substrate and Cofactor[a]

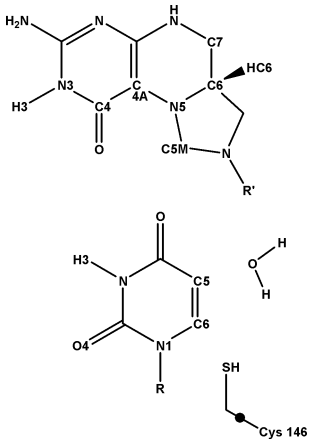

[a] R = 2′-deoxyribose 5′-phosphate, and R′ = PABA glutamate. The link atom is denoted with ●.

inhibitor was replaced with the substrate, the hydrogens were incorporated into the structure to a state complementary to pH 7.5, using DYNAMO (*12*). Since standard pK_a values of ionizable groups can be shifted by local protein environments (*13*), an accurate assignment of the protonation states of all these residues was carried out by recalculating the standard pK_a values of the titratable amino acids using the "cluster method" (*13*), as implemented by Field and coworkers (*14*). According to this method, each titratable residue in the protein is perturbed by the electrostatic effect of the protein environment. Due to the fact that the total charge of the system was not neutral, a sum of 24 sodium counterions was placed in optimal electrostatic positions around the protein (never closer than 10.5 Å from any atom of the system or 5 Å from another counterion, and using a regular grid of 0.5 Å). Then, the system, on its inertia axis, was placed in the mass center of a cavity deleted from a prerelaxed orthorhombic box of water molecules (80 Å × 80 Å × 100 Å). All the water molecules with an oxygen atom lying within 2.8 Å of any heavy atom were removed. The entire chemical system was then divided into a QM region, comprising the cofactor CH_2H_4folate, the substrate dUMP, a portion of the Cys146, and some water molecules (three in the first step and one in those remaining) (see Scheme 3), and a MM region which includes the rest of the system (enzymatic subunits, counterions, and crystallization and solvation water molecules). The methods selected to describe each system were the AM1 (*15*) semiempirical Hamiltonian for the QM region and the OPLS-AA (*16*) and TIP3P (*17*) force fields for the MM region. The link-atom method (*18*, *19*) was used to treat the covalent bond of Cys146 crossing the boundary between the QM and MM regions, to satisfy the valence of the QM fragments (represented by ● in Scheme 3).

Relaxation of the resulting model was performed by means of hybrid QM/MM molecular dynamics (MD). For this purpose, a Langevin bath with a coupling temperature of 293 K was employed throughout this work, using the canonical thermodynamic ensemble (NVT). A total run of 200 ps for the whole system was made with an integration step size of 1 fs. To treat the nonbonding interactions, periodic boundary conditions were applied, using a switch function with a cutoff distance in the range of 16−18 Å.

Afterward, hybrid QM/MM potential energy surface (PES) explorations and stationary-point location and characterization were carried out, guided by the micro-macro iterations scheme (*20*). In this method, the system is divided into two parts, the core or control space, and the environment or complementary space, which is the Hessian matrix calculated explicitly only for those atoms belonging to the core. Once this partitioning has been carried out, stationary-point location (minimum or saddle point) is carried out in the degrees of freedom of the core, under a fully relaxed environment. Thus, before each gradient or Hessian-guided step for the core, the degrees of freedom of the environment are optimized to maintain an approximately zero gradient and to minimize the potential energy. In our case, the core region contained all the QM atoms. Once first-order saddle points (SPs) were located and characterized, subsequent reaction coordinate paths (ESRP or ES1RP) (*21*, *22*) were traced down toward the corresponding minima (reactants, intermediates, or products), followed by a global optimization procedure. Each step of the reaction path was obtained by applying a control/complementary space technique, thus being the gradient vector of the QM atoms computed after complete relaxation of the MM atoms. The difference between this and the true intrinsic reaction coordinate path (IRC), which was traced down from the saddle point to the corresponding minima using the full gradient vector, was trivial since the core was selected so that contributions of atoms outside the core were almost negligible. Also, it was essential to use a small step size in the IRC computation to allow the environment to relax at each step and to prevent the algorithm from halting falsely or from losing the right direction. Due to the size of the system, all the residues more than 20 Å from the active site were kept frozen (54 141 atoms from a total of 62 966 atoms). The conformational changes of the enzymes, as indicated by the X-ray structures of the wild-type enzyme with different ligands (see ref *1* and references therein) and the analysis of the *B* factors for the same enzyme (*23*), also indicated that the relevant conformational fluctuations are within 10 Å of the reaction center. This criterion was extended to the rest of the simulations. The global rms residual gradient in the optimized structures was always less than 0.04 kcal mol^{-1} $Å^{-1}$.

Once the potential energy profiles were obtained for all the chemical steps, a free energy profile, in terms of the potential of mean force (PMF), was calculated for the rate-limiting step using the weighted histogram analysis method (WHAM) combined with the umbrella sampling approach (*24*, *25*), as implemented in DYNAMO. The starting geometry for these calculations was in all cases the saddle-point structure previously located on the PES, while the distinguished reaction coordinate was taken as the antisymmetric combination of the distances describing the breaking and forming bonds, i.e., dCH−dHC, on the hydride transfer step (see step 6 in Scheme 2). This variable was confirmed as being the most representative coordinate changing along the reaction path, thus being the natural choice for determining the PMF. The procedure for the PMF calculation was straightforward and required a series of hybrid QM/MM molecular dynamics simulations in which the reaction coordinate variables were restrained for particular values. The values of the variables sampled during the simulations were then pieced together to construct a full distribution

function from which the PMF was obtained. A total of 80 simulations were performed at different values of the reaction coordinate, with an umbrella force constant of 2500 kJ mol^{-1} $Å^{-1}$ for each particular value. On each window, 5 ps of relaxation MD followed by 20 ps of production was computed. The time step for integrating the equations of motion was chosen (0.5 fs) due to the nature of the chemical step involving a hydrogen transfer. The Verlet algorithm was used to update the velocities.

The rigid-rotor/harmonic-oscillator approximation was used with CAMVIB and CAMISO (*26*, *27*) to calculate the KIEs at 293 K. To obtain averaged values, 10 transition state-like structures were selected as those originated from the 40 ps QM/MM Molecular Dynamics snapshots every 4 ps. These structures were subsequently denoted SP1−SP10, respectively (during the MD trajectory, the reaction coordinate was constrained at the value corresponding to the transition state located on the PES). Afterward, these selected structures were fully optimized as saddle points, and subsequent reaction coordinate paths (ESRP or ES1RP) were traced down toward the corresponding reactants, followed by a global optimization procedure. In common with other vibrational properties such as IR spectroscopic frequencies, isotope effects are local properties (*28*) in the sense that they are determined by the immediate environment of the center of isotopic substitution; this local environment extends by only one or two bond distances ("cutoff rule"). This justifies the fact that the ratios of partition functions were calculated not for the whole enzyme but only for a subset of the full system. In this sense, KIEs were calculated by using the core subset of atoms (equivalent to the QM region) to compute the Hessian matrices in the presence of the environment effect. All force constants and vibrational frequencies were used without scaling in these calculations.

Finally, to overcome the limitations of the selected AM1 semiempirical Hamiltonian, a density functional theory (DFT)-based method was used in our hybrid QM/MM scheme with the aim of obtaining representative results for the rate-limiting step. In this approach, the total potential energy is expressed as a sum of different contributions:

$$E = E_{MM} + \langle \Psi | \hat{H}^0_{DFT} | \Psi \rangle + \sum \frac{q^{FIT}_{QM} Q_{MM}}{r_{QM/MM}} + E^{Lennard-Jones}_{QM/MM} \quad (1)$$

where E_{MM} accounts for the energy of the force field (protein and solvent molecules), Ψ is the QM wave function polarized by the presence of the external electrostatic field due to the classical environment, and $\hat{H}^0_{DFT}$ is the selected gas phase DFT Hamiltonian operator. The last two energy terms are responsible for the QM and MM coupling (Coulombic electrostatic and van der Waals, respectively). Thus, both interaction terms are evaluated classically. The main difference is the way the electrostatic term is obtained. An electrostatic fit for the atomic charges of the QM atoms, using the ChelpG method (*29*), is carried out from the polarized wave function. These charges are introduced later in the classical Coulombic electrostatic potential function between QM and MM regions. This way, only the polarization effect and the gas phase energy come from the DFT/ab initio selected method, while the electrostatic interaction term is reduced to its classical expression. Of course, the difference between the potential energy surfaces (the DFT/ab initio and the classical ones) will rely on the appropriateness of the fitting method: the greater the difference, the longer the optimization will be required to reach convergence.

Furthermore, eq 1 can be expressed in terms of the gradient vector or the Hessian matrix, to be applied in common optimization algorithms. In our work, where a control space/complementary space method was applied, fitted charges of the QM atoms (control space) were kept fixed during all the complementary space (protein and solvent molecules) relaxation, and the Hessian matrix was only recalculated each 10 optimization steps, being updated by means of the Bofill algorithm (*30*) in the rest of the steps. In any case, the time needed to perform an optimization (saddle-point or minimum search) with this method was rather long compared with a standard semiempirical method, and this was the main reason why it was only used for studying the rate-limiting step of the proposed mechanism.

A pure BLYP exchange functional, with a 6-31G* basis set, was selected for the calculations. In addition, the QM region was reduced, due to the large amount of atoms initially present in it, to only the pteridine ring in the case of the folate, and the six-membered ring with the ribose ring in dUMP, comprising a total of 60 atoms instead of the 94 used with the AM1 Hamiltonian.

RESULTS AND DISCUSSION

Potential Energy Surface. A complete exploration of the reaction mechanism for the TS-catalyzed reaction, by means of potential energy surfaces (PESs), was carried out to obtain insight into this complex multistep reaction. Either the proper geometrical variable or a combination of variables was employed as a distinguished reaction coordinate for generating the PES of each step.

The proposed molecular mechanism depicted in Scheme 4 was drawn from the results of all the PESs. Please note that alternative steps (mechanisms) were also tested and resulted in higher barriers.

The molecular mechanism is developed in nine steps, three more steps than the mechanism proposed by Santi and Carreras (*1*). This is due not only to the fact that some of the steps, initially supposed to be concerted-like reactions, take place through stable intermediates but also to a more detailed description of the chemical transformations. The mechanism is as follows. In the first step, Cys146 transfers a hydrogen to a water molecule that acts as a base in an exothermic reaction ($\Delta E \approx -21$ kcal/mol). It is important to point out that our results have revealed that three water molecules, present in the X-ray structure of the protein obtained by Stroud et al. (*9*−*11*), contribute to the transfer of a proton from Cys146 through three transition state structures with a limiting barrier of 5.0 kcal/mol. To confirm the exothermic character of this chemical reaction, which presents a small barrier in the forward direction, this equilibrium step has also been studied in the gas phase and in solution with a very simple molecular model with Gaussian 03 (*31*) (see the Supporting Information). The results show that the protein environment favors, thermodynamically, the transfer of a proton to the water molecule. This confirms the hypothesis of an existing water molecule

Scheme 4: Proposed Molecular Mechanism for the *E. coli* TS-Catalyzed Reaction Obtained from the Multi-AM1/MM PES Exploration[a]

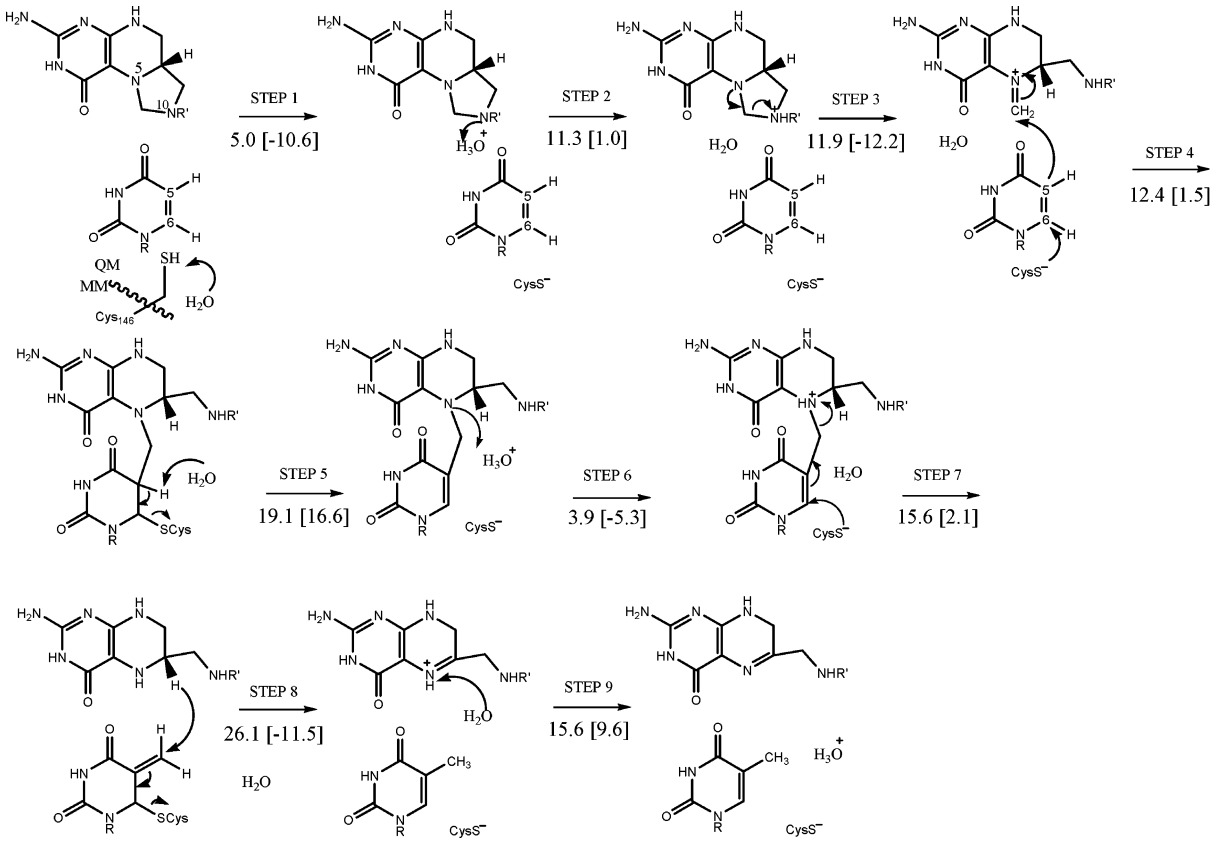

[a] R = 2′-deoxyribose 5′-phosphate, and R′ = PABA glutamate. Activation energy barriers and reaction energies (in brackets) of each step are presented in kilocalories per mole.

that can act as the donor of the proton to the cofactor in the next step. The acid character of this water molecule is probably due to the presence of a negatively charged Glu58, which is within hydrogen bonding distance. This was already proposed by Santi et al. (*1*) and is in accordance with observations showing substantial shifts in the pK_a values of residues in enzyme active sites or otherwise shielded from solvent (*13*, *32*). In fact, calculation of the pK_a of Cys146 in the protein environment rendered a value of 6.7, confirming the observed trend of this residue being slightly more acidic than expected from its standard pK_a value in solution (8.3).

The protonated water molecule acts as a general acid catalyst in step 2, transferring a hydrogen to N10 of the CH_2H_4folate cofactor and facilitating the opening of the imidazolidine ring followed by the formation of the activated form of the cofactor, the iminium ion 5-CH_2H_4folate (steps 2 and 3). The existence of this intermediate in the PES is in agreement with experimental evidence (*33*, *34*).

In the next step (step 4), a nucleophilic attack at C6 of dUMP by the basic deprotonated Cys146 and the concomitant formation of a bond between C5 of dUMP and the iminium ion take place in a concerted way. This covalently bound intermediate has been experimentally isolated by means of quenching techniques (*35*, *36*), which also brings the experimental evidence and our predicted mechanism into agreement. Step 5 is an E2 elimination of the thiol anion (Cys146) at C6 and the proton at C5, forming an intermediate double bond (C5═C6). This description is quite different from the traditional mechanism proposed by Santi et al. (*1*), where the abstraction of the proton at C5 of dUMP takes place concertedly with formation of C4 enol. After a careful inspection of the protein structure, the only general base that can abstract the proton is the water molecule (W40), which is hydrogen bonded to Tyr94 [although the contribution of this Tyr to the induced basicity of the water is not clear (*37*, *38*)]. Any other attempt to use a residue of the protein as the abstracting base has rendered much higher barriers. To test the commonly proposed enol formation at the C4 carbonyl, we calculated the "traditional" path and proved that it was energetically much less favorable (by 35.3 kcal/mol) than the proposed step 5. This result suggests a breaking of the bond established between Cys146 and dUMP through C6. This is in accordance with the experimental findings of Montfort et al. (*9*−*11*). It also shows an electron density for C6 more diffuse than for the other atoms in the pyrimidine ring, thus suggesting that the instability of the nucleotide−Cys146 thiol adduct may assist in abstraction of a proton from dUMP. The following step (step 6) involves the protonation of N5 (folate) that turns the tetrahydropterin into a much better leaving group.

Afterward, the formation of the protonated pyrazine ring facilitates the scission of the methylene bridge established between the substrate and the cofactor, which takes place with a concomitant trans-diaxial nucleophilic attack of the negatively charged Cys46 on C6 of the folate (step 7). This concerted step leads to the elimination of H_4folate and to the cleavage of the covalent bond between the pteridine ring and the exo-methyline dUMP intermediate, the existence of which is supported by studies of model reactions (*5*, *39*). Steps 4−7 are substantially different from the commonly

proposed elimination of proton and H_4folate from the C5−C7 bond. Traditionally, this step is proposed to be initiated by abstraction of a proton from C5 and an anion intermediate stabilized by the enolic system and H-bonds to the carbonyl O═C4 group (*40*, *41*). Our calculations indicate that such an abstraction of hydrogen from C5, without elimination of the thioester bond at C6, would take place with an energy barrier of 35.5 kcal/mol, which is much higher than that of our newly proposed mechanism.

Subsequently, the favorable three-dimensional orientation of the pterin ring of the cofactor and the pyrimidine of the substrate prepares the system for a transfer of hydride from H_4folate to dUMP in step 8, releasing the Cys146 in a single concerted but very asynchronous step. This step (step 8) presents the highest potential energy barrier (26.1 kcal/mol) of all the PESs that were studied, which is in agreement with the fact that this hydride transfer corresponds to the rate-limiting step of the full enzyme-catalyzed process. In the final step (step 9), a water molecule abstracts the remaining proton of the H_4folate to restore the H_2folate.

Therefore, our calculated PESs have allowed us to propose a full molecular mechanism, compatible with experimentally deduced evidence. This indicates that the transfer of hydride from the cofactor to the substrate is the rate-determining step, in agreement with experimental studies. Hence, we will focus our attention in the future on this step. A note of caution has to be introduced at this point, since the quantum Hamiltonian used to describe the breaking and forming bonds is the semiempirical AM1 and semiempirical methods can overestimate the barriers. In this regard, a very expensive relocalization of the transition structure of step 8 was carried out at the BLYP/MM level, followed by an IRC and a full optimization of reactants and products. The resulting potential energy profiles rendered an energy barrier of 8.2 kcal/mol, which was dramatically smaller than the AM1/MM one (26.1 kcal/mol). This value is now in accordance with the expected order of magnitude for a biologically catalyzed chemical reaction. Although BLYP/MM calculations have not been carried out for every step of the mechanism (due to computer time limitations), similar corrections to the rest of the steps are expected to reduce the barriers by equivalent amounts. Consequently, extremely expensive BLYP/MM calculations would not change the trend between the AM1-calculated activation energy barriers, and the hydride transfer step would still be the rate-limiting one. Furthermore, the optimized geometries of the reactants and transition state for this step are comparable to the ones obtained by means of the AM1/MM method. These results validate, to some extent, the PESs obtained with the semiempirical/MM approach and provide a reliable global picture of the new proposed mechanism, notwithstanding the overestimated values of the activation barriers.

Potential of Mean Force. To obtain more accurate results for the rate-limiting step, directly comparable with experimentally determined data, the free energy profile of step 8 was calculated in terms of the potential of mean force (PMF). The profile describes an exothermic chemical reaction, −9.0 kcal/mol, with an activation free energy of 28.8 kcal/mol. This result appears to be reasonable from the thermodynamic point of view, since an exothermic reaction was expected, although the barrier for an enzymatically catalyzed reaction appears to be overestimated. As mentioned above, a possible source of error is the use of the AM1 semiempirical Hamiltonian. Then, a correction term, defined as the difference between the potential energy barriers obtained at a low level and a high level of theory (AM1/MM − DFT/MM), has been added. The resulting activation free energy was reduced to 10.9 kcal/mol, a value which is significantly closer to that deduced from the experimentally measured rate constant by Kohen et al. at 293 K (4.0 ± 0.1 kcal/mol) (*2*). Nevertheless, this experimental measurement is complicated by the temperature dependence substrate inhibition and reflects an activation energy on a rather complex kinetic term.

Table 1: Averaged Distances (angstroms) and Dihedral Angles (degrees), Related to the Substrate and Cofactor, Obtained at the Reactants and Transition State of the Rate-Limiting Hydride Transfer Step of the TS-Catalyzed Reaction, Computed at the AM1/MM Level of Theory

	reactants	transition state
C6(folate)−HC6(folate)	1.1363 ± 0.0005	1.276 ± 0.013
HC6(folate)−C5M(UMP)	2.64 ± 0.13	1.504 ± 0.019
C6(folate)−C5M(UMP)	3.67 ± 0.12	2.770 ± 0.009
C6(UMP)−SG(Cys146)	2.4 ± 0.3	3.4 ± 0.3
N5(folate)−C5(UMP)	4.3 ± 0.3	3.37 ± 0.10
C4A(folate)−C6(UMP)	4.55 ± 0.19	3.64 ± 0.10
C4(folate)−N1(UMP)	4.44 ± 0.15	3.991 ± 0.06
N3(folate)−C1′(UMP)	3.97 ± 0.04	3.87 ± 0.03
N5(folate)−C6(folate)−C5M(UMP)−C5(UMP)	−8.0 ± 3.0	−7.87 ± 1.12
C5M(UMP)−C6(folate)−C7(folate)−N3(folate)	−88.0 ± 1.7	−100.7 ± 1.3
HG(Ser54)−O2(folate)	1.916 ± 0.024	1.91 ± 0.03
HZ3(Lys48)−OE1(folate)	1.77 ± 0.03	1.76 ± 0.03
OD2(Asp169)−H3(folate)	2.489 ± 0.014	2.463 ± 0.015
H1(Wat40)−SG(Cys146)	1.79 ± 0.03	1.734 ± 0.08
HH11(Arg166)−SG(Cys146)	1.79 ± 0.07	1.615 ± 0.020
HH22(Arg166)−O3P(UMP)	1.600 ± 0.008	1.613 ± 0.008
HD22(Asn177)−O4(UMP)	2.08 ± 0.08	1.949 ± 0.018
OD1(Asn177)−H3(UMP)	2.386 ± 0.018	2.372 ± 0.009
OE1(Glu58)−H2(Wat11)	1.84 ± 0.03	1.788 ± 0.012
OE2(Glu58)−H2(Wat11)	2.84 ± 0.08	2.67 ± 0.04
HH(Tyr94)−OH2(Wat40)	1.791 ± 0.020	1.774 ± 0.012
HH21(Arg21)−O5′(UMP)	1.82 ± 0.19	1.824 ± 0.018
HE(Arg21)−O1P(UMP)	1.712 ± 0.010	1.693 ± 0.013

An extensive conformational analysis of the geometries of the transition state, as well as the reactants of the rate-limiting step (step 8), at the AM1/MM level was carried out. We added a parabolic potential to the reaction coordinate at the corresponding value of the transition state and ran molecular dynamic simulations. As explained in Computational Methods, 10 different transition state structures were optimized, and their corresponding IRCs were traced down to reactant valleys until complete relaxation of the structures was achieved. Several geometrical variables of both states, corresponding to the substrate−cofactor, substrate−protein, or cofactor−protein interactions, are listed in Table 1. A representative snapshot of the transition state structures of the rate-limiting step is depicted in Figure 1 (a stereoview of Figure 1 is presented as Supporting Information).

The first conclusion that can be drawn from the analysis of the averaged geometrical data of Table 1 is that the hydride transfer takes place at an almost invariable conformation of the substrate and cofactor. The donor and acceptor rings are almost parallel and in an endo conformation (see the dihedral angles listed in Table 1). With regard to the interatomic distances established between the substrate or the cofactor and the residues in the active site of the protein, it can be

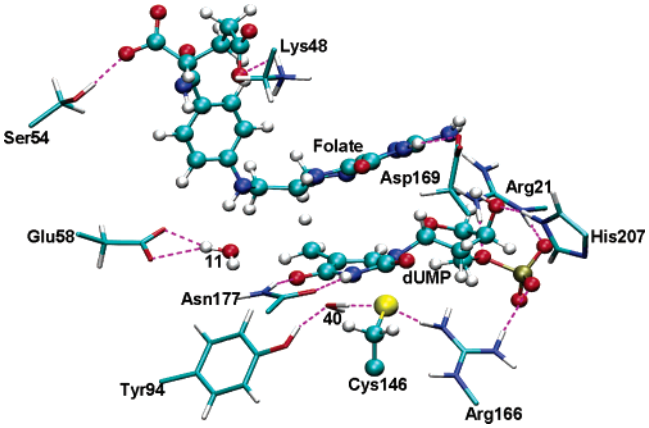

FIGURE 1: Representative structure of the transition state of the rate-limiting hydride transfer step located in the active site of the TS enzyme, computed at the AM1/MM level of theory.

observed that the electron donor residues are closer to the folate in the transition state than in reactants, while electron acceptor residues approach the dUMP. This result is reasonable considering that a negative charge is being transferred from the cofactor and, thus, the negatively charged residues are stabilizing the more positive folate, while positively charged residues are stabilizing the more negative dUMP ring at the transition state. This global movement of the residues in the active site of the protein should facilitate the hydride transfer and stabilize the transition state.

Kinetic Isotope Effects. As mentioned in the introductory section, the physical nature of the hydride transfer step in the TS has been extensively studied by means of isotope effects. Particularly interesting are the data corresponding to the primary deuterium and tritium kinetic isotope effects (KIEs). These data are extremely useful as they render direct information about the transition state in a particular chemical step. Furthermore, they can be compared with theoretical calculations. For this purpose, the 10 different located and refined transition state structures, together with their corresponding reactants (linked by each reaction path), were selected to compute KIEs for the substitution of the transferred hydride with deuterium and tritium. Secondary α-deuterium KIEs and heavy atom KIEs for the sulfur atom of the Cys146 were also computed. The results are listed in Table 2, where a semiclassical correction of the tunneling effect has been computed by means of the Bell equation (*42*, *43*). It is relevant to point out that dynamic features of the rate process are removed from consideration and the equilibrium nature of transition state theory is preserved. Nevertheless, it is interesting to note that Bigeleisen and Wolfsberg showed that the quantum mechanical nature of the reaction coordinate could be directly incorporated into the theory, and in doing so, they arrived at the truncated form of the Bell equation (*44*). For a complete analysis of the results, interatomic distances of the three atoms involved in the forming and breaking bonds (as well as the distance between the thiol sulfur atom of Cys146 and the C5 atom of dUMP and the energy barriers of the 10 transition state structures) are listed in Table 3. DFT/MM-computed primary and secondary KIEs are listed in Table 4, together with the corresponding potential energy barriers and their imaginary frequencies.

Table 2: Primary and Secondary Kinetic Isotope Effects for the Hydride Transfer Step of the TS-Catalyzed Reaction Computed from 10 Different AM1/MM Optimized Saddle-Point Structures[a]

	^{2}H primary KIE	^{3}H primary KIE	^{34}S primary KIE	^{2}H secondary KIE
SP1	3.89	7.07	1.00110	0.9643
SP2	5.14	10.42	1.00284	0.9110
SP3	3.71	6.63	1.00072	0.9784
SP4	3.57	6.28	1.00071	0.9821
SP5	3.76	6.75	0.99985	0.9847
SP6	3.73	6.68	0.99906	0.9355
SP7	3.99	7.32	0.99854	0.9733
SP8	3.91	7.11	0.99909	0.9342
SP9	4.06	7.51	1.00014	0.9735
SP10	4.20	7.85	1.00081	0.9677
arithmetic average	4.0 ± 0.3	7.4 ± 0.7	1.0003 ± 0.0008	0.960 ± 0.016
energy-weighted average	3.990 ± 0.005	7.319 ± 0.011	0.998540 ± 0.000010	0.9733 ± 0.0007
experimental	3.72 ± 0.12[b]	6.91 ± 0.05[c]	–	0.89 ± 0.05[d]

[a] Averages are also presented, as well as the experimental KIEs. [b] From ref *45*. [c] From ref *2*. [d] From ref *38*.

Table 3: Interatomic Distances (angstroms), Energy Barriers (kilocalories per mole), and Imaginary Frequencies (inverse centimeters) of the 10 Transition State Structures Optimized at the AM1/MM Level of Theory

	C6(folate)−HC6(folate)	HC6(folate)−C5M(UMP)	antisymmetric combination	C6(UMP)−SG(Cys146)	imaginary frequency	$\Delta E^{\ddagger}$
SP1	1.271	1.491	−0.220	3.07	1067.37i	26.9
SP2	1.330	1.441	−0.111	2.47	1421.68i	31.6
SP3	1.265	1.507	−0.242	3.23	1019.86i	23.1
SP4	1.259	1.521	−0.262	3.35	980.53i	25.3
SP5	1.263	1.541	−0.278	3.64	992.54i	27.8
SP6	1.260	1.548	−0.288	3.98	995.62i	21.2
SP7	1.276	1.505	−0.229	3.77	1131.77i	17.0
SP8	1.275	1.501	−0.226	3.77	1105.95i	22.3
SP9	1.280	1.487	−0.206	3.44	1140.96i	27.9
SP10	1.283	1.498	−0.215	3.48	1172.51i	37.8
average	1.276 ± 0.013	1.504 ± 0.019	−0.23 ± 0.03	3.4 ± 0.3	1102.88i	26 ± 4

Table 4: Energy Barriers (kilocalories per mole), Interatomic Distances (angstroms), and Imaginary Frequencies (inverse centimeters) of the Transition State Structures Optimized at the BLYP/6-31G*/MM Level of Theory[a]

$\Delta E^{\ddagger}$	8.22
imaginary frequency	880.14i
C6(folate)−HC6(folate)	1.355
HC6(folate)−C5M(UMP)	1.391
antisymmetric combination	−0.036
C6(UMP)−SG(Cys146)	2.248
^{2}H primary KIE	5.139
^{3}H primary KIE	10.441
^{34}S primary KIE	1.0035
^{2}H secondary KIE	0.979

[a] Primary and secondary kinetic isotope effects for the hydride transfer step correspond to the rate-limiting step of the TS-catalyzed reaction.

The first conclusion that can be derived from the information provided in Table 3 is that important deviations are observed in the energy barriers. As observed, the energy barriers range from 17.0 to 37.8 kcal/mol. This result can be related to previous theoretical (*46*−*52*) and experimental (*53*, *54*) studies on different enzyme reactions, where a wide dispersion of rate constants can be observed in single-molecule experiments, each corresponding to different reaction paths. Our findings demonstrate, once again, the need to carry out extensive conformational analysis when systems of a huge number of degrees of freedom are being studied. From a geometric point of view, the transition state structures are comparable. The antisymmetric combination of the breaking and forming bonds defining the hydride transfer appears to be quite robust (−0.23 ± 0.03 Å). Furthermore, it is important to point out that the IRC traced down from the 10 saddle points to their respective reactants reveals that no intermediate was located, although the bond between the sulfur atom of Cys146 and the C6 atom of dUMP was almost broken, as deduced by the carbon−sulfur distance and its contribution to the eigenvector of the Hessian. This asynchronicity is not so evident in the SP2, where the values defining the reaction coordinate and the distance defining the separation of Cys146 change in a more concerted way.

Information presented in Table 2 shows that primary KIEs are normal. These results are in very good agreement with the experimental studies of Spencer et al. (*45*), Agrawal et al. (*2*), and Hong et al. (*38*). This agreement justifies the assumption that the hydride transfer is indeed the rate-limiting step of the full enzymatic mechanism, validating, to some extent, the proposed molecular mechanism. The secondary deuterium KIEs are inverse, and their value is related to the negative value of the reaction coordinate at the transition state (the antisymmetric combination presented in Table 3). This means that the hydride transfer is at an early stage of the process; the orbital hybridization on the accepting carbon atom (C5M UMP) at the transition state is closer to sp^2 than to the final sp^3. As listed in Table 2, the arithmetic averaged secondary deuterium KIE is 0.960 ± 0.016, while the experimental value is 0.89 ± 0.05. Thus, the theoretical prediction is almost within the experimental uncertainty (0.976−0.944 for the former and 0.94−0.84 for the latter).

The heavy atom KIE, although not yet measured experimentally, is almost equal to unity, in accordance with little participation of the carbon−sulfur breaking bond in the transition vector of this saddle point. Another interesting result is observed in the transition state structure SP2: this saddle point presents an unusually short carbon−sulfur distance. Obviously, a more concerted character of the transition structure is also related to higher KIEs, especially the heavy atom KIE (a value of 1.0028 is obtained for SP2 while the averaged KIE is 1.0003, as shown in Table 2). This structure, together with SP10, exhibits the highest energy barrier which, in principle, means that a chemical path through this transition state structure should present a very low weight in an energy-weighted average of all the possible paths. Nevertheless, we must keep in mind the fact that energies reported in Table 3 correspond to energy barriers, while absolute energies should be considered in a proper Bolztmann population analysis.

Finally, from the results reported in Table 4, we can observe that the barrier of the rate-limiting step, computed at the DFT/MM level, is significantly lower than the one obtained at the AM1/MM level, as expected. As for the KIEs, the much more expensive BLYP/6-31G* method employed to describe the QM region does not dramatically change the results, nor are the conclusions derived from the AM1/MM calculations. It seems that KIEs are more sensitive to the slightly different geometries obtained for the transition state structures than to the known overestimated frequencies rendered by the semiempirical Hamiltonian (880.14i and 1102.88i cm^{-1} for BLYP and AM1, respectively). This is probably due to the cancellation of errors when the vibrational partition functions of the reactants and transition state are computed. Thus, by comparison of the data reported in Tables 2 and 4, DFT/MM KIEs are quite close to the values obtained at the AM1/MM level for the SP2 transition state structure, which is the AM1/MM transition state geometry that is the closest to the high-level DFT/MM (see interatomic distances of SP2 reported in Table 3 and the corresponding distances in Table 4). This result justifies, partially, the reliability of the overall mechanism obtained at a lower level of theory.

CONCLUSIONS

In this paper, we present a theoretical study of the molecular mechanism of the reaction catalyzed by thymidylate synthase. The hybrid quantum mechanics/molecular mechanics (AM1/OPLS/TIP3P) technique that was used has allowed inclusion of the protein environment and exploration of structural features of significance on potential energy hypersurfaces spanning several thousands of degrees of freedom. We have characterized the transition state structures describing each step in the full mechanism, which has allowed definition of the role of the different amino acids and water molecules in the process. After the different energy barriers had been evaluated, the hydride transfer step appears to be the rate-limiting step, in agreement with experimental observations. Higher-level DFT/MM calculations were employed to recalculate the potential energy profile of the hydride transfer, demonstrating the influence of the quality of the Hamiltonian in the computed energies: AM1/MM rendered a much higher energy barrier than BLYP/MM. To obtain more plausible results, the free energy profile of the rate-limiting step was computed in terms of the PMF. The free energy barrier, considering the correction term of the semiempirical AM1 Hamiltonian, is in accordance with the

expected magnitude of the enzymic process. Furthermore, once the free energy profile was obtained, molecular dynamic simulations were calculated for the reactants and the transition state to relocate slightly different conformers representative of both states. The comparison of 10 different transition state structures, together with their corresponding 10 different reactant species, shows that, while some common features are observed, for reactions involving a large number of degrees of freedom, it is not accurate to refer to them as a unique transition structure. The transition state should be considered as an energy-weighted average of nearly degenerated transition structures, which can exhibit non-negligible differences. These differences are understood from the geometrical point of view and, obviously, also from their energetics and their KIEs. Good agreement has also been obtained between experimental and our averaged semiclassical QM/MM primary deuterium and tritium KIEs and secondary deuterium KIEs. Furthermore, heavy atom ^{34}S KIE calculations for the thiol sulfur atom of Cys146 reveal that the hydride transfer takes place with a concomitant breaking of the bond between C6 of the substrate and Cys146. This latter bond is, on average, almost broken at the transition state. A simple arithmetic average of the 10 reaction paths renders primary deuterium and tritium KIEs of 4.0 ± 0.3 and 7.4 ± 0.7, respectively, values which are very close to the experimental estimations of the KIEs (3.72 ± 0.12 and 6.91 ± 0.05, respectively).

A general conclusion that emerges from the existence of the different calculated reaction paths is that molecular dynamics simulations are always required to correctly sample the most contributing energy paths using a Boltzmann distribution of saddle points along the dividing line. Such molecular dynamics calculations are important in any attempt to obtain significant free energy profiles and reliable geometrical analysis, which in turn may allow prediction of the role of the active site residues and design of the transition state analogue inhibitors.

From the mechanistic point of view, several substantial differences between previously proposed mechanisms (based mostly on organic chemistry intuition) and our new molecular mechanism are apparent. The role of protonation of carbonyl 4 and stabilization of enol intermediates throughout the path is challenging. At the same time, the calculations suggest that the C−S bond at the C6 position of dUMP is very labile. Consequently, the elimination of the H_4folate (steps 5−7) involves transit cleavage of the C−S bond with little assistance from tautomerization of the C4 carbonyl. Likewise, the findings suggest that the nucleophilic attacks on C6 and the iminium carbon (step 4) are concerted and that hydride transfer occurs when the C−S bond is almost fully cleaved (with the exception of one of the optimized transition state structures). The findings bear a possible impact on the design of mechanism-based inhibitors and drugs. For example, in the design of dUMP-based inhibitors, attention should be focused on trapping the thioether formed in the Michael addition (step 4) rather than in the stabilization of the C5−C4−O4 system.

ACKNOWLEDGMENT

We acknowledge the Servei d'Informàtica of the Universitat Jaume I for providing us with computer capabilities. We thank M. Kanaan for reading the manuscript and the useful suggestions.

SUPPORTING INFORMATION AVAILABLE

Stereoview of Figure 1 (Figure S1) and reaction energies corresponding to the equilibrium between CH_3SH and H_2O calculated by means of ab initio HF/6-31G* methods in the gas phase and in solution with a polarizable continuum model (Table S1). This material is available free of charge via the Internet at http://pubs.acs.org.

REFERENCES

1. Carreras, W. C., and Santi, D. V. (1995) The catalytic mechanism and structure of thymidylate synthase, *Annu. Rev. Biochem. 64*, 721−762.
2. Agrawal, N., Hong, B., Mihai, C., and Kohen, A. (2004) Vibrationally enhanced hydrogen tunneling in the *Escherichia coli* thymidylate synthase catalyzed reaction, *Biochemistry 43*, 1998−2006.
3. Friedkin, M. (1959) in *The kinetics of cellular proliferation* (Stohlman, F. J., Ed.) Grune and Stratton, New York.
4. Santi, D. V., and Pogolotti, A. L. (1968) Oxygen-alkyl ester cleavage of 5-acetoxymethyl uracils, *Tetrahedron Lett.*, 6159−6162.
5. Santi, D. V., and Brewer, C. F. (1968) Model studies of thymidylate synthetase. Neighboring-group facilitation of electrophilic substitution reactions of uracil furanosides, *J. Am. Chem. Soc. 90*, 6236−6238.
6. Santi, D. V., and Brewer, C. F. (1973) Model studies of thymidylate synthetase. Intramolecular catalysis of 5-hydrogen exchange and 5-hydroxymethylation of 1-substituted uracils, *Biochemistry 12*, 2416−2424.
7. Pogolotti, A. L., and Santi, D. V. (1974) Model studies of the thymidylate synthetase reaction. Nucleophilic displacement of 5-p-nitrophenoxymethyluracils, *Biochemistry 13*, 456−466.
8. Santi, D. V., McHenry, C. S., and Sommer, H. (1974) Mechanism of interaction of thymidylate synthetase with 5-fluorodeoxyuridylate, *Biochemistry 13*, 471−481.
9. Montfort, W. R., Perry, K. M., Fauman, E. B., Finer-Moore, J. S., Maley, G. F., Hardy, L., Maley, F., and Stroud, R. M. (1990) Structure, multiple site binding, and segmental accommodation in thymidylate synthase on binding dUMP and an anti-folate, *Biochemistry 29*, 6964−6977.
10. Finer-Moore, J. S., Montfort, W. R., and Stroud, R. M. (1990) Pairwise specificity and sequential binding in enzyme catalysis: Thymidylate synthase, *Biochemistry 29*, 6977−6986.
11. Perry, K. M., Fauman, E. B., Finer-Moore, J. S., and Montfort, W. R. (1990) Plastic adaptation toward mutations in proteins: Structural comparison of thymidylate synthases, *Proteins: Struct., Funct., Genet. 8*, 315−333.
12. Field, M. J. (1999) *A practical introduction to the simulation of molecular systems*, Cambridge University Press, Cambridge, U.K.
13. Antosiewicz, J., McCammon, J. A., and Gilson, M. K. (1994) Prediction of pH-dependent properties of proteins, *J. Mol. Biol. 238*, 415−436.
14. Field, M., David, L., and Rinaldo, D. (2006) personal communication.
15. Dewar, M. J. S., Zoebisch, E. G., Healy, E. F., and Stewart, J. J. P. (1985) Development and use of quantum mechanical molecular models. 76. AM1: A new general purpose quantum mechanical molecular model, *J. Am. Chem. Soc. 107*, 3902−3909.
16. Kaminiski, G. A., Friesner, R. A., Tirado-Rives, J., and Jorgensen, W. L. (2001) Evaluation and reparametrization of the OPLS-AA force field for proteins via comparison with accurate quantum chemical calculations on peptides, *J. Phys. Chem. B 105*, 6474−6487.
17. Jorgensen, W. L., Chandrasekhar, J., Madura, J. D., Impey, R. W., and Klein, M. L. (1983) Comparison of simple potential functions for simulating liquid water, *J. Chem. Phys. 79*, 926−935.
18. Warshel, A., and Levitt, M. (1976) Theoretical studies of enzymic reactions− Dielectric, electrostatic and steric stabilization of carbonium-ion in reaction of Lysozyme, 415−436. *J. Mol. Biol. 103*, 227−249.

19. Singh, U. C., Kollman, P. A., and Karplus, M. (1986) A combined ab initio quantum mechanical and molecular mechanical method for carrying out simulations on complex molecular systems: Applications to the $CH_3Cl + Cl^-$ exchange reaction and gas phase protonation of polyethers, *J. Comput. Chem. 7*, 718−730.
20. Martí, S., Moliner, V., and Tunon, I. (2005) Improving the QM/MM description of chemical processes: A dual level strategy to explore the potential energy surface in very large systems, *J. Chem. Theory Comput. 1*, 1008−1016.
21. Fukui, K. (1970) Formulation of the reaction coordinate, *J. Phys. Chem. 74*, 4161−4163.
22. Melissas, V. S., Truhlar, D. G., and Garrett, B. C. (1992) Optimized calculations of reaction paths and reaction-path functions for chemical reactions, *J. Chem. Phys. 96*, 5758−5772.
23. Newby, Z., Lee, T. T., Morse, R. J., Liu, Y. Q., Liu, L., Venkatraman, P., Santi, D. V., Finer-Moore, J. S., and Stroud, R. M. (2006) The role of protein dynamics in thymidylate synthase catalysis: Variants of conserved 2′-deoxyuridine 5′-monophosphate (dUMP)-binding Tyr-261, *Biochemistry 45*, 7415−7428.
24. Kumar, S., Bouzida, D., Swendsen, R. H., Kollman, P. A., and Rosenberg, J. M. (1992) The weighted histogram analysis method for free-energy calculations on biomolecules. 1. The method, *J. Comput. Chem. 13*, 1011−1021.
25. Torrie, G. M., and Valleau, J. P. (1977) Non-physical sampling distributions in Monte-Carlo free-energy estimation-umbrella sampling, *J. Comput. Phys. 23*, 187−199.
26. Williams, I. H. (1982) On the representation of force fields for chemically reacting systems, *Chem. Phys. Lett. 88*, 462−466.
27. Williams, I. H. (1983) Force-constant computations in Cartesian coordinates. Elimination of translational and rotational contributions, *THEOCHEM 94*, 275−284.
28. Sühnel, J., and Schowen, R. L. (1991) *Enzyme mechanism from isotope effects*, CRC Press, Boca Raton, FL.
29. Breneman, C. M., and Wiberg, K. B. (1990) Determining atom-centered monopoles from molecular electrostatic potentials. The need for high sampling density in formamide conformational analysis, *J. Comput. Chem. 11*, 361−373.
30. Fletcher, R. (1987) *Practical methods of optimization*, Wiley, New York.
31. Frisch, M. J., Trucks, G. W., Schlengel, H. B., Scuseria, G. E., Robb, M. A., Cheeseman, J. R., Zakrzewski, V. G., Montgomery, J. A., Jr., Stratman, R. E., Burant, J. C., Dapprich, S., Millam, J. M., Daniels, A. D., Kundin, K. N., Strain, M. C., Farkas, O., Tomasi, J., Barone, V., Cossi, M., Cammi, R., Mennucci, B., Pomelli, C., Adamo, C., Clifford, S., Ochterski, J., Petersson, G. A., Ayala, P. Y., Cui, Q., Morokuma, K., Malick, D. K., Rabuck, A. D., Raghavachari, K., Foresman, J. B., Ciolowski, J., Ortiz, J. V., Stefanov, B. B., Liu, G., Liashebko, A., Piskorz, P., Komaromi, I., Gomperts, R., Martin, R. L., Fox, D. J., Keith, T., Al-Laham, M. A., Peng, C. Y., Nanayakkara, A., Gonzalez, C., Challacombe, M., Grill, P. M. W., Johnson, B., Chen, W., Wong, M. W., Andres, J. L., Head-Gordon, M., Replogle, E. S., and Pople, J. A. (1998) *Gaussian*, Gaussian, Inc., Pittsburgh, PA.
32. Gilson, M. K. (1993) Multiple-site titration and molecular modeling − 2 rapid methods for computing energies and forces for ionizable groups in proteins, *Proteins: Struct., Funct., Genet. 15*, 266−282.
33. Pogolotti, A. L., Ivanetich, K. M., Sommer, H., and Santi, D. V. (1976) Thymidylate synthetase: Studies on the peptide containing covalently bound 5-fluoro-2′-deoxyuridylate and 5,10-methylenetetrahydrofolate, *Biochem. Biophys. Res. Commun. 70*, 972−978.
34. Bellisario, R. L., Maley, G. F., Galivan, J. H., and Maley, F. (1976) Amino acid sequence at the FdUMP binding site of thymidylate synthetase, *Proc. Natl. Acad. Sci. U.S.A. 73*, 1848−1852.
35. Moore, M. A., Ahmed, F., and Dunlap, R. B. (1986) Trapping and partial characterization of an adduct postulated to be the covalent catalytic ternary complex of thymidylate synthase, *Biochemistry 25*, 3311−3317.
36. Huang, W. D., and Santi, D. V. (1994) Isolation of a covalent steady-state intermediate in glutamate 60 mutants of thymidylate synthase, *J. Biol. Chem. 269*, 31327−31329.
37. Climie, S., Ruiz-Perez, L., Gonzalez-Pacanowska, D., Prapunwattana, P., and Cho, S. W. (1990) Saturation site-directed mutagenesis of thymidylate synthase, *J. Biol. Chem. 265*, 18776−18779.
38. Hong, B., and Kohen, A. (2006) unpublished data.
39. Santi, D. V., and Pogolotti, A. L. (1971) Nucleophilic substitution reactions of 5-Acetoxymethyl- and 5 para nitrophenoxymethyluracils, *Heterocycl. Chem. 8*, 265−272.
40. Finer-Moore, J. S., Santi, D. V., and Stroud, R. M. (2003) Lessons and conclusions from dissecting the mechanism of a bisubstrate enzyme: Thymidylate synthase mutagenesis, function, and structure, *Biochemistry 42*, 248−256.
41. Stroud, R. M., and Finer-Moore, J. S. (2003) Conformational dynamics along an enzymatic reaction pathway: Thymidylate synthase, "the movie", *Biochemistry 42*, 239−247.
42. Bell, R. P. (1959) The tunnel effect correction for parabolic potential barriers, *Trans. Faraday Soc. 55*, 1−4.
43. Bell, R. P. (1980) *The tunnel effect in chemistry*, Chapman and Hall, London.
44. Bigeleisen, J., and Wolfsberg, M. (1953) Temperature Independent Factor in the Relative Rates of Isotopic 3 Center Reactions, *J. Chem. Phys. 21*, 1972−1974.
45. Spencer, H. T., Villafranca, J. E., and Appleman, J. R. (1997) Kinetic scheme for thymidylate synthase from *Escherichia coli*: Determination from measurements of ligand binding, primary and secondary isotope effects, and pre-steady-state catalysis, *Biochemistry 36*, 4212−4222.
46. Ferrer, S., Tuñón, I., Marti, S., Moliner, V., Garcia-Viloca, M., González-Lafont, A., and Lluch, J. M. (2006) A theoretical analysis of rate constants and kinetic isotope effects corresponding to different reactant valleys in lactate dehydrogenase, *J. Am. Chem. Soc. 128*, 16851−16863.
47. Turner, J. A., Moliner, V., and Williams, I. H. (1999) Transition-state structural refinement with GRACE and CHARMM: Flexible QM/MM modelling for lactate dehydrogenase, *Phys. Chem. Chem. Phys. 6*, 1323−1331.
48. Min, W., English, B. P., Luo, G. B., Cherayil, B. J., Kou, S. C., and Xie, X. S. (2005) Fluctuating enzymes: Lessons from single-molecule studies, *Acc. Chem. Res. 38*, 923−931.
49. Antikainen, N. M., Smiley, R. D., Benkovic, S. J., and Hammes, G. G. (2005) Conformation coupled enzyme catalysis: Single-molecule and transient kinetics investigation of dihydrofolate reductase, *Biochemistry 44*, 16835−16843.
50. Tan, W. H., and Yeung, E. S. (1997) Monitoring the reactions of single enzyme molecules and single metal ions, *Anal. Chem. 69*, 4242−4248.
51. Thorpe, I. F., and Brooks, C. L. (2005) Conformational substates modulate hydride transfer in dihydrofolate reductase, *J. Am. Chem. Soc. 127*, 12997−13006.
52. English, B. P., Min, W., van Oijen, A. M., Lee, K. T., Luo, G. B., Sun, H. Y., Cherayil, B. J., Kou, S. C., and Xie, X. S. (2006) Ever-fluctuating single enzyme molecules: Michaelis-Menten equation revisited, *Nat. Chem. Biol. 2*, 87−94.
53. Xue, Q. F., and Yeung, E. S. (1995) Differences in the chemical reactivity of individual molecules of an enzyme, *Nature 373*, 681−683.
54. Ansari, A., Berendzen, J., Bowne, S. F., Frauenfelder, H., Iben, I. E. T., Sauke, T. B., Shyamsunder, E., and Young, R. D. (1985) Protein states and proteinquakes, *Proc. Natl. Acad. Sci. U.S.A. 82*, 5000−5004.

BI061953Y